Analysis of the Stator Winding Fault of Induction Motor Using COMSOL Multiphysics

Stanislav Kocman, Stanislav Nowak
Department of Electrical Engineering
VŠB – Technical University of Ostrava
Ostrava, Czech Republic
stanislav.kocman@vsb.cz, stanislav.nowak.st@vsb.cz

***Abstract*—Three-phase induction motors are widely used in the industrial sector. Even if their construction is rather simple resulting in high reliability, some unexpected faults can occur during their operation. Among them, the stator winding faults belong to the most common failures. In this paper, the simulation has been carried out for stator coil–to–ground fault using COMSOL Multiphysics software. This failure causes highly unbalanced stator currents causing changes in rotor currents, motor inner torque, speed, etc. Some simulation results are presented and discussed in this paper.**

Keywords—induction motor, model, simulation, stator currents, stator faults

I. Introduction

Three-phase induction motors are in common use in various technical applications in industrial and tertiary sectors including electric drives (pumps, fans, conveyors, machine tools, reeling machines…), lifts, cranes, machinery, robotics, manufacturing lines, transportation etc. Even if their construction is rather simple resulting in high reliability, some unexpected faults can occur during their operation. A failure of an induction motor e.g. in a manufacturing line resulting in its breakdown can cause high economic waste. Therefore, their monitoring, regular maintenance and diagnostics are very important [1]-[5].

In induction motors various types of failures can occur during their operations, such as a failure of power supply, failures of rotor cage and stator winding, rotor touch on stator, a failure of insulation system, a failure of bearings or a failure of fan [6]-[8]. To the most common faults belong stator winding failures (35-40 % of induction motor breakdowns), and bearing failures (c. the same percentage of motor breakdowns) [9]-[11].

The stator winding faults are associated with the stator winding insulation. They can be initiated by an insulation breakdown between two turns in the same phase (inter–turn short or turn–to–turn short), between coils of the same phase (coil–to–coil short), between two phases (phase–to–phase short) and between one phase to earth (coil–to–ground short). These failures cause current unbalance resulting in high current in the affected phase with an influence on remaining phases [12]. This high current unbalance is accompanied by thermal stresses responsible for the degradation of the stator winding insulation and electrodynamic stresses with an impact on end winding bonding and stator wedging deteriorating the reliability of the motor. It is worth noting that the life span of the stator winding insulation is lessened by c. 50% for 10^0 raise over the insulation temperature limit. The meant 10^0 raise is caused by the permanent current reaching c. 105% of the nominal one.

This work was supported by the SGS FEI, VŠB-TU Ostrava under Grant No SP 2019/65.

II. Mathematical Model of Induction Motor

In the induction motor, two magnetic fields are presented, the first one excited by currents in three-phase stator circuit, the second one by currents in the rotor circuit. There is an electromagnetic coupling between them in the machine. Due to their interaction, the motor inner torque is produced. Some simplified assumptions are accepted, such as sinusoidal, balanced currents creating resultant sinusoidal magnetic field, stator and rotor slotting effects are neglected, linear material of motor iron with neglected losses, spatially symmetrical distributed windings, equal resistances and inductances in each phase, constant air–gap, to create motor mathematical model.

The basic differential equations for the model of induction motor are derived e.g. in [13]-[15]. In the stator coordinate system, the voltage equation is for one phase as follows:

$$\boldsymbol{v}_S = R_S \boldsymbol{i}_S + \frac{\mathrm{d}\boldsymbol{\psi}_S}{\mathrm{d}t}, \tag{1}$$

where $\boldsymbol{v}_S$ is the stator voltage spatial vector, $\boldsymbol{i}_S$ is the stator current, R_S is the stator resistance, $\boldsymbol{\psi}_S$ is the stator flux linkage.

In the rotor coordinate system, the voltage equation is for one phase as follows:

$$\boldsymbol{v}_R = R_R \boldsymbol{i}_R + \frac{\mathrm{d}\boldsymbol{\psi}_R}{\mathrm{d}t}, \tag{2}$$

where $\boldsymbol{v}_R$ is the rotor voltage spatial vector, $\boldsymbol{i}_R$ is the rotor current, R_R is the rotor resistance, $\boldsymbol{\psi}_R$ is the rotor flux linkage.

The flux linkages in (1) and in (2), respectively, are defined as:

$$\boldsymbol{\psi}_S = L_S \boldsymbol{i}_S + L_m \boldsymbol{i}_R e^{\mathrm{j}\omega t}, \tag{3}$$

$$\boldsymbol{\psi}_R = L_R \boldsymbol{i}_R + L_m \boldsymbol{i}_S e^{-\mathrm{j}\omega t}, \tag{4}$$

978-1-7281-1334-0/19/$31.00 ©2019 IEEE

where L_S is the total stator inductance depending on self–inductance of the phase and mutual inductance of stator phases, L_m is the mutual inductance of stator and rotor, ω is the rotor angular velocity, L_R is the total rotor inductance depending on self–inductance of the phase and mutual inductance of rotor phases.

Motor inner electromagnetic torque is defined as:

$$\tau = \frac{3}{2} p \mathrm{I_m}\{\boldsymbol{i}_S \boldsymbol{\psi}_S^*\}, \tag{5}$$

$$\tau = J\frac{\mathrm{d}\omega}{\mathrm{d}t} + \tau_L, \tag{6}$$

where p is the number of the pole pairs, J is the moment of inertia, τ_L is the load torque.

The equations are written in the nature reference frame. To have the mathematical model simpler, the transformations are used, which convert the three-phase system into two-phase system. By means of them, the coordinate system can be fixed to stator, or to rotor, and or the coordinates are rotating with the synchronous speed [14].

As seen from the equations stated above, there is the coupling between the currents in the motor windings and flux linkages. If a fault in stator winding occurs resulting in a current change in the affected phase, so this change is accompanied by changes of flux linkages in the machine causing changes of currents in remaining health phases. These changes bring a change of motor inner electromagnetic torque with an impact on motor mechanical speed.

In this paper, the coil–to–ground short in the stator winding is taken into consideration and adopted for a motor simulation model. The supply voltages of nominal RMS values are sinusoidal and balanced with nominal frequency. The stator winding is connected into star. The fault is assumed in the middle of one phase as seen in Fig. 1. Stator currents and their distribution in phases, inner electromagnetic torque and mechanical speed of the induction motor are simulated and studied using COMSOL Multiphysics software.

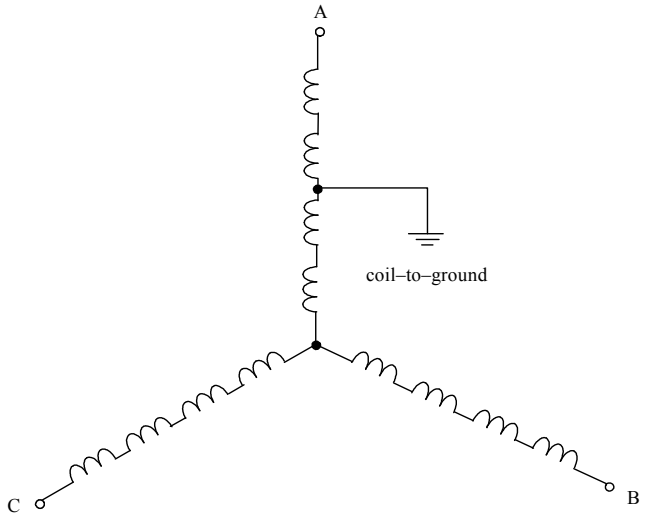

Fig. 1. Stator winding fault (coil–to–ground)

III. Simulation Model of Induction Motor

To simulate the stator winding fault and its consequences the model of the induction motor has been carried out using COMSOL Multiphysics software. The catalogue parameters of the tested motor are shown in Table I.

TABLE I. The Selected Parameters of Motor

Parameter	Value	Parameter	Value
Rated power	4 kW	Nom. power factor	0.83
Nominal voltage	400 V	Nominal speed	1440 rpm
Nominal current	8.4 A	Nominal torque	27 N·m
Nominal frequency	50 Hz	Nominal efficiency	83.1 %

The model was designed as two-dimensional with defined out of plane thickness [16]-[18]. To design geometry, materials, parameters, connections and transient processes physics and interfaces of COMSOL have been used such as Geometry and Material physics, Rotating Machinery, Magnetic interface, Electrical Circuit interface and Global ODE and DAE interface [19]. The Rotating Machinery, Magnetic physical interface under the COMSOL AC/DC Module enables solving the magnetic field in the machine using equations defined by the formulas:

$$\sigma\frac{\partial \boldsymbol{A}}{\partial t} + \nabla\times\boldsymbol{H} - \sigma\boldsymbol{v}\times\boldsymbol{B} = \boldsymbol{J}_e, \tag{7}$$

$$\nabla\times\boldsymbol{A} = \boldsymbol{B}, \tag{8}$$

where σ is the electric conductivity, $\boldsymbol{A}$ is the magnetic vector potential, $\boldsymbol{H}$ is the magnetic field intensity, $\boldsymbol{v}$ is the velocity of conductors, $\boldsymbol{B}$ is the magnetic flux density, $\boldsymbol{J_e}$ is the externally generated current density.

For the stator slots, the multi-turn coil domains were used, where the externally generated current density $\boldsymbol{J_e}$ is defined as:

$$\boldsymbol{J}_e = \frac{NI}{A}\boldsymbol{e}, \tag{9}$$

where N is the number of turns of the stator coil, I is the stator phase current, A is the total cross-section area of the stator coil domain, $\boldsymbol{e}$ is the vector field representing the direction of the wires in the stator slot.

The rotor slots are defined using single-turn coil domains, where the externally generated current density for the time-dependent study is defined as:

$$\boldsymbol{J}_e = \sigma\frac{V}{d}\boldsymbol{e}, \tag{10}$$

where V is the electrical potential applied on the turn of the coil, i.e. on the rotor bar, d is the out of plane physics thickness.

The motor inner torque $\boldsymbol{\tau}$ computed by the integration of the Maxwell's stress tensor over the exterior surfaces of the set of domains is defined as:

$$\boldsymbol{\tau} = \oint_{\partial\Omega} d(\boldsymbol{r}-\boldsymbol{r}_0)\times(\boldsymbol{n}T)\mathrm{d}S, \tag{11}$$

where Ω is set of domains involving domains in the rotor, shaft and the half of the motor air gap, $\boldsymbol{r}$ is the position vector, $\boldsymbol{r}_0$

is the torque rotation point, $\boldsymbol{n}$ is the outward normal from the surface, T is the stress tensor, dS represents the differential boundary length.

Starting induction motor in a drive assembly is a transient process, which is described by the fundamental torque equation, or the equation of motion, as defined by (6). To simulate the motor start-up the modified motion equation is used in the Global ODEs and DAEs interface of COMSOL formulated as:

$$\tau = J\frac{\mathrm{d}^2\alpha}{\mathrm{d}t^2} + \tau_L, \tag{12}$$

where α is the rotation angle.

The external electrical circuits have been modelled in Electrical Circuit interface with parameters defined in [20].

To design the model in COMSOL, the manufacturer's layouts of the stator and rotor sheets were used. The simulated values depend on the accuracy of geometry of motor iron sheets.

This induction motor model has been verified by comparing its results to results from experimental measurements, to motor catalogue parameters, or to the theoretical presumptions, respectively [21]-[22].

IV. Simulation Results

The simulation has been carried out for the motor with the parameters listed in Table I. The motor was started–up with the load equal to the nominal torque. The start-up is accompanied by high starting stator currents and oscillations in the motor inner torque, which correspond to them in motor speed. After time c. 0.35 s the motor reaches its steady–state with speed equal to 1437.8 rpm. In Fig. 2, the induction motor geometry is shown illustrating the magnetic flux density distribution and equipotential lines of the magnetic vector potential. The waveforms of the stator currents drawn by the motor from the source is in Fig. 3, the inner electromagnetic torque is shown in Fig. 4 and the motor speed in Fig. 5. As seen from the courses the coil–to–ground short in one phase of the stator winding occurs after reaching the motor steady–state.

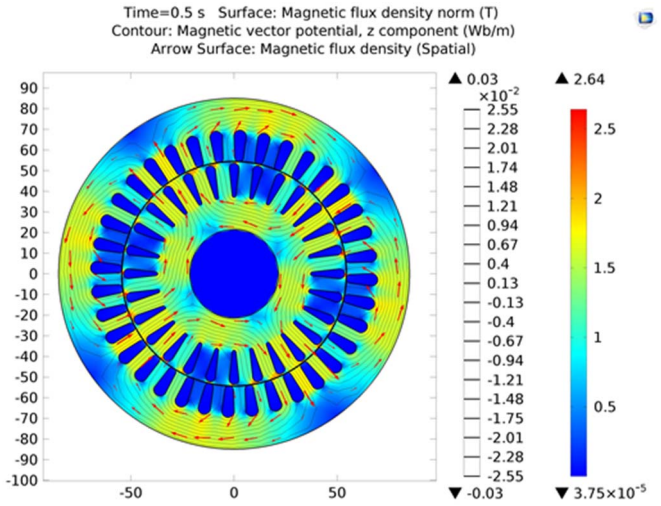

Fig. 2. Magnetic flux density and equipotential lines of magnetic vector potential

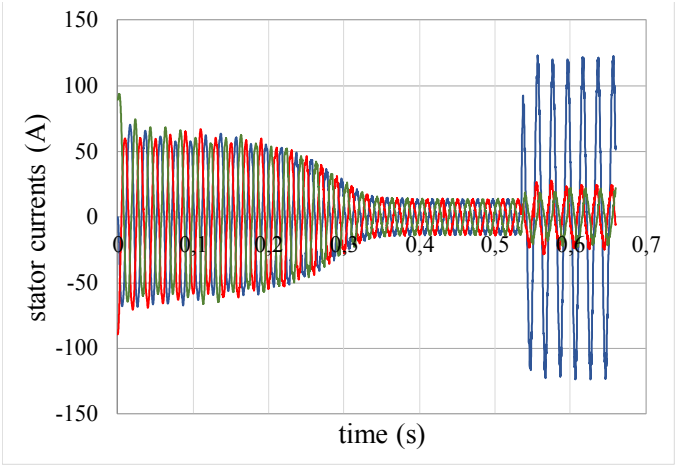

Fig. 3. Waveforms of stator currents

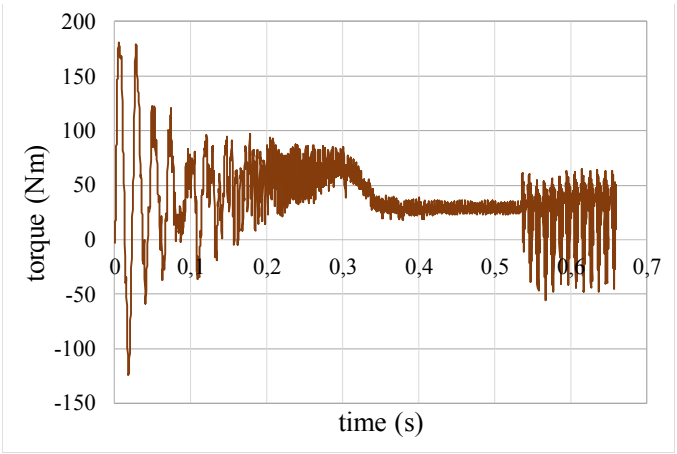

Fig. 4. Waveform of inner torque

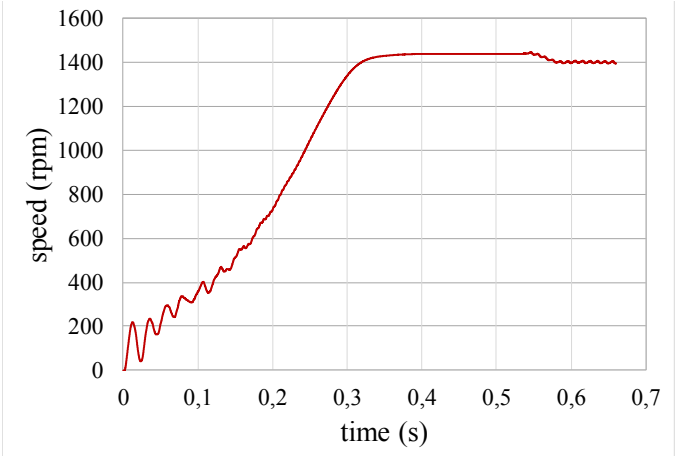

Fig. 5. Waveform of speed

Detailed waveforms of stator currents after reaching the steady state are shown in Fig. 6. From the harmonic analysis of the currents, the first harmonics were detected. Their values for each phase are listed in Table II. In Fig. 7, the detailed course of the motor inner torque together with its mean value is shown in Fig. 8. The mean value magnitude can be seen in Table II.

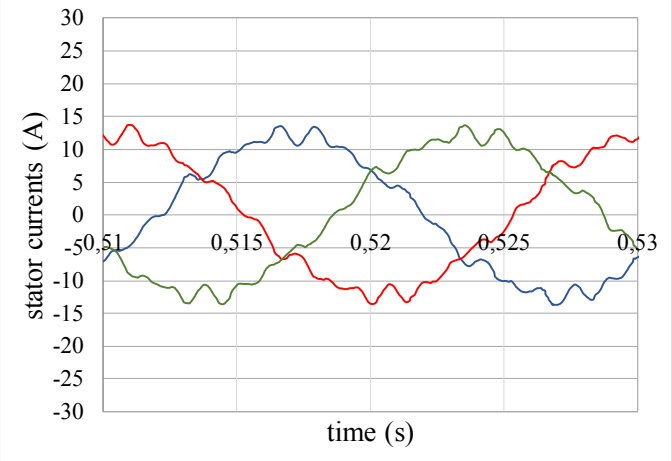

Fig. 6. Waveforms of stator currents from Fig. 3 for one period

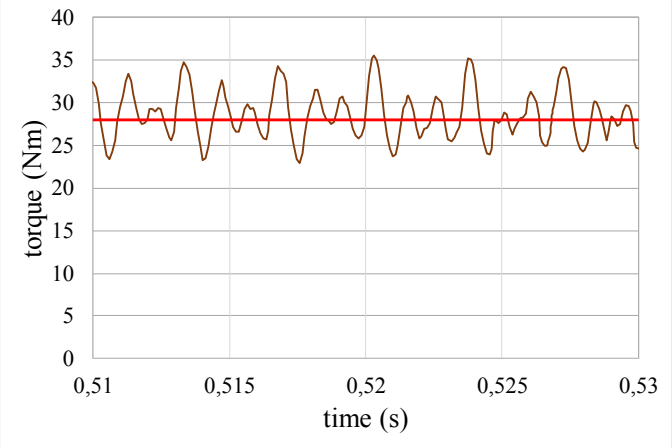

Fig. 7. Waveform of inner torque and its mean value

The coil–to–ground short causes a change of the balanced system into an unbalanced one resulting in high current in the affected phase with an influence on currents of remaining phases. The stator currents have an impact on magnetic flux in the machine iron and change its magnitude and waveform. The symmetrical magnetic field in the motor iron as seen in Fig. 2 converts into a non–symmetrical field as can be seen in Fig. 8, with different distribution of magnetic flux density and magnetic vector potential in stator and rotor sheets. Whereas under the motor health condition the rotating magnetic field is circular with constant total magnetic flux amplitude, under the failure mode the rotating magnetic field is not circular anymore with changes of the total magnetic flux amplitude.

The more detailed stator currents waveforms after the coil–to–ground short are shown in Fig. 9. As seen, after a short transient a new steady–state is reached, but with very high current unbalance both amplitude and phase. The current distortion is also evidently increased. To compare the steady–state before and after occurring of the coil–to–ground short, the course of the first current harmonics are shown in Fig. 10, and in Fig. 11, respectively. The current RMS values, their initial phases and total harmonic distortion THD_i are presented in Table III.

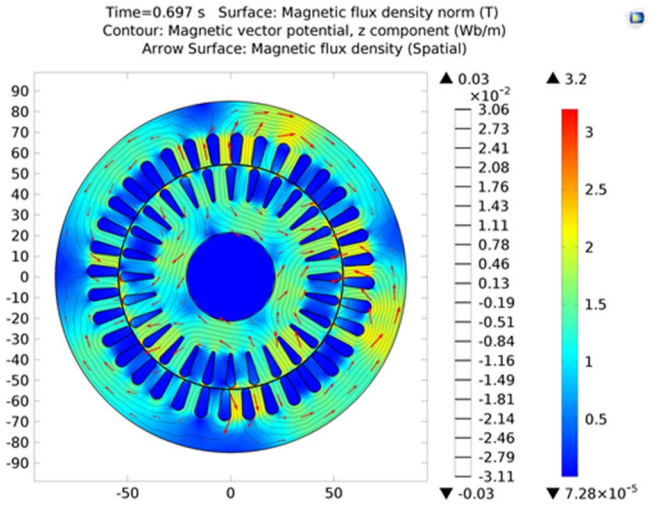

Fig. 8. Magnetic flux density and equipotential lines of magnetic vector potential under the failure mode

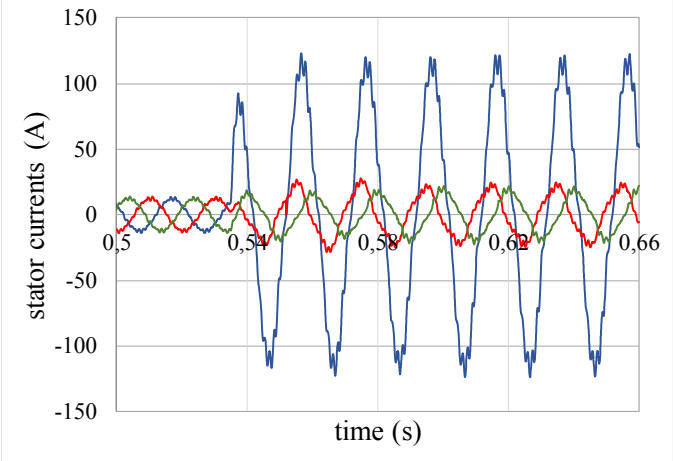

Fig. 9. Waveforms of stator currents after the coil–to–ground short failure

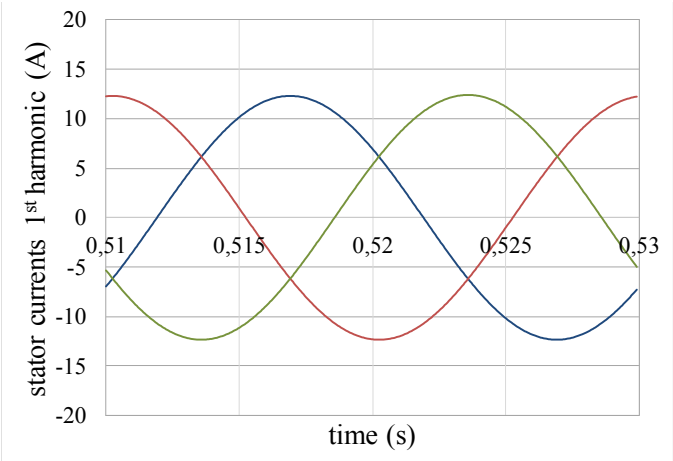

Fig. 10. Waveforms of stator currents 1st harmonic before the coil–to–ground short failure

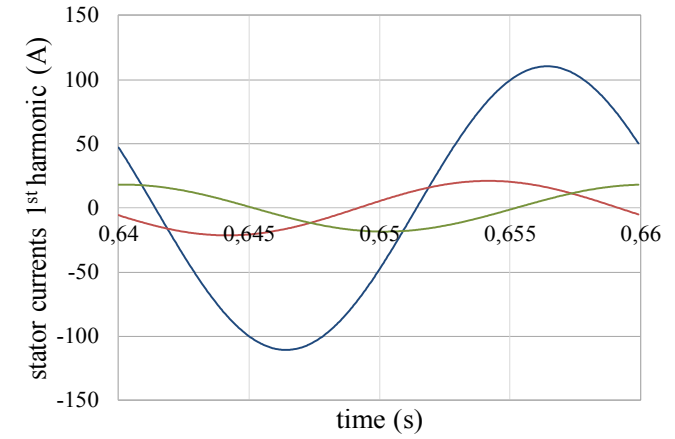

Fig. 11. Waveforms of stator currents 1st harmonic after the coil–to–ground short failure

In Fig. 12, the waveform of motor inner torque after the failure is shown. In comparison to Fig. 7 the high oscillations in the inner torque course can be seen, which are associated with the increased drawn current in the affected phase. However, its mean value magnitude is very close to this of the health condition as it can be seen in Table II.

In Fig. 13, the motor speed after the failure is shown.

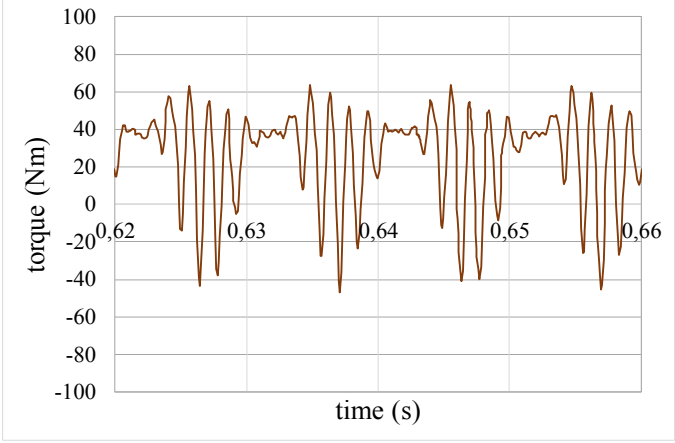

Fig. 12. Waveform of inner torque after the coil–to–ground short failure

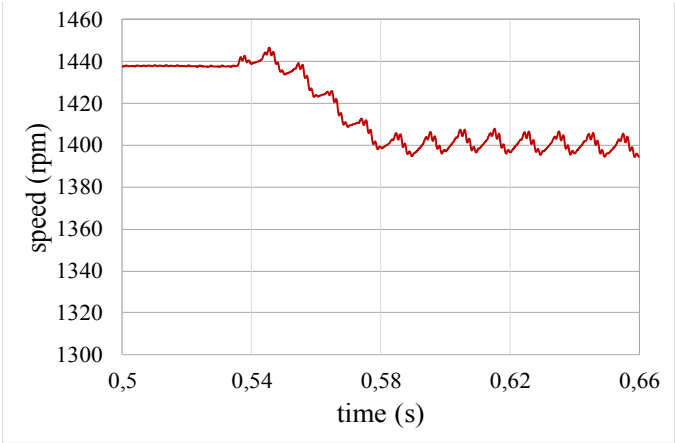

Fig. 13. Waveform of speed after the coil–to–ground short failure

When the failure occurs, the speed drops to a new decreased value. The oscillations in the motor inner torque cause corresponding oscillations in the speed waveform. The speed mean value before and after the failure is also presented in Table II.

TABLE II. THE MONITORED PARAMETERS

	Stator currents			Inner torque	Speed
	I_A (A)	I_B (A)	I_C (A)	τ (N·m)	n (rpm)
Before fault	8,73	8,74	8,72	27,7	1437,8
After fault	78,2	12,9	15,1	26,9	1400,2

TABLE III. THE STATOR CURRENTS CHARACTERISTICS

	Before fault			After fault		
	RMS (A)	*phase* (^{0})	THD_i (%)	*RMS* (A)	*phase* (^{0})	THD_i (%)
Phase A	8,73	-34,2	5,7	78,2	154,7	7,7
Phase B	8,74	-154,3	5,8	12,9	86,7	9,4
Phase C	8,72	85,7	5,8	15,1	195,1	13,5

V. CONCLUSION

The simulation of the stator coil–to–ground short failure has been carried out. It confirmed the high unbalance of drawn currents. As seen in Table III the state after the fault is profoundly different from the state before the fault. The difference among the stator currents is very high, with current unbalance reaching the value of 120,9%. The phase shift between two currents is not equal to 120 degrees as at the balanced system, but quite different. The current distortion represented by total harmonic distortion THD_i is higher at the state after failure, and with the differences in individual phases in comparison to the state before failure.

As regards the motor inner torque and speed whose mean values are shown in Table II, the difference can be seen in their waveforms when the state after fault is accompanied by high oscillations. The mean value of speed drops down to the value shown in Table II.

As seen from the results of the stator coil–to–ground short simulation, this failure causes high currents in stator windings when the current in the affected phase is higher than the motor starting current.

REFERENCES

[1] Y. B. Koca, and A. Unsal, "A rewiev on detection and monitoring of stator faults of induction motors," International Journal of Innovative Research in Science, Engineering and Technology, vol. 6, iss. 10, pp. 70–74, May 2017.

[2] S. Karmakar, S. Chattopadhyay, M. Mitra, and S. Sengupta, Induction Motor Fault Diagnosis. Singapore: Springer-Verlag, 2016, pp.7–28.

[3] A. Ukil, S. Chen, and A. Andenna, "Detection of stator short circuit faults in three-phase induction motors using motor current zero crossing instants," Electric Power Systems Research, No. 81, vol. 4, pp. 1036–1044, April 2011.

[4] M. O. Mustafa, On Fault Detection, Diagnosis and Monitoring for Induction Motors. Luleå University of Technology, 2015.

[5] H. Guzman, I. Gonzalez, F. Barrero, and M. Durán, Induction Motors - Applications, Control and Fault Diagnostics. London: IntechOpen, 2015.

[6] S. K. Ahamed, Fault Diagnosis of Three Phase Induction Motor. University of Calcutta, 2016.

[7] K.K. Pandey, P.H. Zope, and S.R. Suralkar, “Review on fault diagnosis in three-phase induction motor,” International Journal of Computer Applications, vol. 1, pp. 53–58, Sep. 2012.

[8] L. Varshney, S. Jovanovic, J.S. Shakya, and R.K. Saket, “Performance and reliability evaluation of induction machines: an overview,” International Journal of Research and Review in Applied Sciences, vol. 8, No. 1, pp. 104–108, Jul. 2011.

[9] A. P. Ompusunggu, Z. Liu, H. D. Ardakani, C. Jin, F. Petre, and J. Lee, “Winding fault diagnosis of a 3-phase induction motor powered by frequency-inverter drive using the current and voltage signals,” Proceedings of the 14th Mechatronics Forum International Conference, Mechatronics, pp. 182–189, Jun. 2014.

[10] S.M.Shashidhara, “Stator winding fault diagnosis of induction motor using FFT,” International Journal of Advance Engineering and Research Development, vol. 4, iss. 10, pp. 816–826, Oct. 2017.

[11] A. A. Obed, “Detection, protection from, classification, and monitoring electrical faults in 3-phase induction motor based on discrete S-transform,” International Journal of Applied Engineering Research, vol. 13, iss. 9, pp. 6690-6699, 2018.

[12] P. Kadaník, O. Červinka, and J. Ryba, Causal Model of Induction Motor for Stator Diagnostics. Rockwell Automation, Prague, 2000.

[13] J. Měřička, and Z. Zoubek, Teorie obecného elektrického stroje. ČVUT Praha, 1982.

[14] E. Thoendel, Simulační model asynchronního stroje, FEL ČVUT Praha, 2008.

[15] M. Konuhova, G. Orlovskis, K. Ketners, “Mathematical modelling of induction motor transient processes during stator winding interruption,“ Scientific Journal of Riga Technical University, vol. 27, pp. 73–76, 2010.

[16] J. Martinez, A. Belahcen, and A. Arkkio, “A 2D FEM model for transient and fault analysis of induction machines,“ Przeglad Elektrotechniczny, vol. 88, No. 7B, pp. 157–160, Jul. 2012.

[17] V. N. Savov, Zh. D. Georgiev, and E. S. Bogdanov, “Analysis of cage induction motor by means of the finite element method and coupled system of field, circuit and motion equations,“ Electrical Engineering, vol. 80, pp. 21–28, Feb. 1997.

[18] S. Kocman, P. Pečínka, and T. Hrubý, “Induction motor modelling using COMSOL Multiphysics,“ 17th International Scientific Conference on Electric Power Engineering, Prague, pp. 408–412, May 2016.

[19] COMSOL AC/DC Module User's Guide, 2015.

[20] S. Kocman, T. Hrubý, P. Pečínka, and A. Neumann, “FEM model of asynchronous motor for analysis of its parameters,“ 11th IEEE International Conference~ELEKTRO, Strbske Pleso, pp. 315-319, Sep. 2016.

[21] S. Kocman, P. Orság, and P. Pečínka, “Simulation of start-up behaviour of induction motor with direct online connection,“ Advances in Electrical and Electronic Engineering, vol. 15, No. 5, pp. 754–762, Dec. 2017.

[22] S. Kocman, P. Orság, and P. Pečínka, “Simulation of selected induction motor operating conditions using COMSOL software,“ Advances in Electrical and Electronic Engineering, vol. 16, No. 3, pp. 288–296, Sep. 2018.